TIPP 2011 - Technology and Instrumentation for Particle Physics 2011

Temperature Dependence of Charge Carrier Properties in Single Crystal CVD Diamond Detectors

Hendrik Jansen[1],[a], Daniel Dobos[a], Vladimir Eremin[b], Heinz Pernegger[a], Norbert Wermes[c]

[a]*CERN, 1211 Genve 23, Switzerland*
[b]*Ioffe Technical Institute, 26 Polytekhnicheskaya, St Petersburg 194021, Russian Federation*
[c]*University of Bonn, Regina-Pacis-Weg 3, 53113 Bonn, Germany*

Abstract

Single crystal chemical-vapour deposition (scCVD) diamonds are interesting for a wide range of applications. For many of them a good understanding of the temperature dependence of charge carrier transport mechanisms and properties is crucial. Measurements on the temperature dependence of charge carrier movement in scCVD diamond semiconductor detectors are presented. The evolution of the pulse shape of the detector response from impinging α particles is measured as a function of temperature employing the α-induced transient current technique (α-TCT) within a temperature range from 67 K to 295 K. The measurements are used to extract the drift mobility, drift velocity, and saturation velocity, in terms of which the results are interpreted.

Keywords: scCVD Diamond, charge carrier properties, temperature dependence, transient current technique, TCT, drift mobility, drift velocity

1. Introduction

Diamond is becoming more and more popular as a detector material, as its usability increases with improving production techniques in terms of higher charge collection efficiency (CCE) and lower impurity density. Amongst others the two LHC experiments CMS [1] and ATLAS [2] and also the LHC machine [3] itself operate Beam Conditions Monitors [4],[5] and Beam Loss Monitors [6] with chemical-vapour deposition (CVD) diamond as the sensor material. Both, single crystal and polycrystalline CVD (scCVD, pCVD) sensors are used as they are radiation hard materials with a displacement energy of 43 eV [7]. Diamond has exceptional electrical properties [8]. Its large band gap (5.47 eV) results in a high breakdown field ($> 1 \times 10^7$ V/cm) — allowing for high-field operation — and a very low leakage current ($\lesssim 2$ pA for $|U| < 400$ V) which renders very precise signal current measurements possible. A disadvantage is the high average electron-hole pair creation energy (~ 13.5 eV) leading to smaller signal currents in comparison to silicon devices. However, a low dielectric constant ($\epsilon = 5.7$) reduces relatively the sensor capacitance and

---

[1]Corresponding author: jansen@cern.ch

hence the noise in comparison to silicon ($\epsilon = 11.9$). Signal-to-noise ratios of diamond based detectors are often comparable to silicon devices, depending on electronics. However, especially in detector grade scCVD diamond free charge carriers have long trapping times (≥ 30 ns).

During the last 40 years, the transient current technique (TCT) has frequently been used in order to determine the charge carrier mobility and velocity in different materials. In insulators, it was used in 1970 by Lampert and Mark [9]. Later, the TCT was further developed for the measurement of effective net charge in the space charge region of p-n junction detectors [10]. Pernegger et al. carried out TCT measurements using α particles for carriers excitation (α-TCT) in order to determine charge carrier properties in scCVD diamond at room temperature (RT) [11]. A study for a variety of semiconductor materials, namely for CdTe, CZT, silicon p-in-n diodes, as well as two scCVDs, has been performed by Fink et al. [12]. Also photon-induced TCT studies have been done with scCVD samples making use of a 5x-frequency multiplied Nd-YAG laser [13].

In the literature drift mobility values for both carrier types, electrons and holes, in scCVD diamond samples vary significantly. Drift mobility values have been reported at ~ 2300 cm^2/Vs for holes and ~ 1700 cm^2/Vs for electrons using α-induced currents [11], and 2000 to 2250 cm^2/Vs for holes and 2200 to 2750 cm^2/Vs for electrons using laser induced currents [14]. Isberg et al. report a hole mobility value as high as $\mu_h = (3400 \pm 400)$ cm^2/Vs [13].

While charge carrier properties in diamond have been studied with various samples at room temperature (RT) and higher, their temperature dependence towards LHC cold mass temperatures (1.9 K) needs to be studied in more detail.

In this paper we employ the method of α-TCT measurement at various temperatures and extract the temperature dependence of charge carrier properties in a detector-grade scCVD diamond. A cryostat is used to control the sample temperature in a region from 295 K down to 67 K. The electric field strength is varied from 0.2 V/μm to 1.2 V/μm. Exploiting the detector response for various bias voltages and temperatures, we measure the transit time values for electron and holes and derive the temperature dependence of drift velocity, saturation velocity, and low-field drift mobility.

2. Experimental Technique

2.1. Transient Current Technique

The α-TCT provides a unique way of deriving drift mobility and drift velocity with a single measurement. α-TCT measurements are usually performed in a metal-semiconductor-metal structure and use the measurement of time-resolved currents induced on a read-out electrode by the drift of free charge carriers in an electric field. The free carriers are created close to the sensor surface by an α source. As the charges drift through the semiconductor bulk, the recorded signal pulse shape is sensitive to its material properties. If the current is read with large bandwidth, charge carrier properties can be derived accurately from pulse characteristics. With charge carrier trapping times τ_{trap} exceeding the time a charge needs to drift through the bulk, i.e. the transit time t_t, and with charge carrier creation limited to a small depth in comparison to the bulk thickness, the transit time can readily be calculated from the difference in time between rising and falling edge. In present scCVD diamonds trapping times larger than 30 ns are realised [11]. Short depth of penetration is realised by using highly ionizing α particles from an Am-241 source. Bragg-simulations based on NIST data [15] show a penetration depth of ~ 10 μm for a α particle energy of 4.7 MeV, which is small compared to common sample thicknesses of several hundred microns. By measuring the transit time it is possible to calculate the average drift velocity and the drift mobility. Measurements in a wide range of electric field strength can be used to determine the low-field mobility and the saturation velocity.

2.2. Sample

The sample under test (SUT), which we refer to as *S57* for later reference, has been produced with a chemical-vapour deposition process by Diamond Detector Ltd (DDL) [16]. It consists of a scCVD diamond with a sample area of 4.7×4.7 mm^2 and a sample thickness of 500 μm. The dislocation and impurity densities are of the order of $\leq 2 \times 10^{14}$ cm^{-3}. DDL quotes a nitrogen incorporation of < 1 ppb. The SUT is equipped

with metal contacts on both sides. The leakage current is smaller than $7\,\mathrm{pA}$ for $U = \pm600\,\mathrm{V}$. According to the specifications from the manufacturer, the contacts are made from three layers: DLC^2/Pt/Au with $\sim$ 4/10/200 nm thicknesses, respectively. The metallised area is quadratic, has a surface of $4.2 \times 4.2\,\mathrm{mm}^2$, and does not include a guard ring. DDL quotes a CCE > 95% at $1\,\mathrm{V/\mu m}$. The diamond's sample capacitance is measured to be $C_{\mathrm{d}} = (2 \pm 0.3)\,\mathrm{pF}$ with an HP Agilent 4263B. This value is in good agreement with the theoretical value of $C_{\mathrm{d}}^{\mathrm{th}} = \epsilon\epsilon_0 \frac{A}{d} = 1.78\,\mathrm{pF}$.

2.3. Measurement Set-up

An existing set-up, described in [17], has been used and slightly modified to fit our needs. A helium-gas Stirling cooler provides cooling and a system of pumps produce a vacuum. All presented measurements have been performed at $< 1 \times 10^{-4}$ mbar in order to avoid heat conduction. The diamond sample is placed on top of a ceramic plate with gold contacts that penetrate the plate. They provide the electrical contact between the bias line and the bottom contact of the diamond. The ceramic plate features good thermal conductivity in order to provide direct and constant cooling of the diamond sample. It is arranged on top of a copper finger, which is cooled via the Stirling cooler. On top of the diamond a plastic collimator of $70\,\mu\mathrm{m}$ thickness is placed. The aperture is $2\,\mathrm{mm}$ in diameter. Thereby it is ensured that α particles from the Am-241 source impinge the detector only within the metallised area. A sketch of the cross section of the set-up is shown in Fig. 1 (left).

An Am-241 source with aluminium packaging is located at $1.5\,\mathrm{mm}$ distance to the diamond's grounded top electrode. The electrical schematics of the set-up is shown in Fig. 1 (right). The HV is applied at the bottom contact. The amplifier is AC-coupled to the HV line via a 1 nF capacitor. As electron-hole (e-h) pairs are created close to the top contact, one type of charge carrier is collected almost immediately at the top contact, whilst the other drifts through the whole bulk to reach the bottom contact. Hole (electron) induced currents are read if a negative (positive) bias voltage is applied to the bottom contact. The bias is provided by a Keithley 2410. The α source has an activity of roughly $40\,\mathrm{kBq}$ resulting in a particle flux of $< 100\,\mathrm{s}^{-1}$ for the chosen collimator size. Polarization effects are thus avoided. In order to cross-check non-occurrence of polarization effects, pulses have been compared for different radiation durations of the diamond. The carrier transit time measured after one minute and after ten minutes of radiation agree within $< 1\%$.

The α particles emitted from the Am-241 source have an energy of $5.4\,\mathrm{MeV}$. The source is sealed with a palladium layer of $1.8\,\mu\mathrm{m}$ thickness. Taking into account the sealing and the metallisation of the SUT, the α particles reach the bulk with $4.7\,\mathrm{MeV}$, producing a maximum of 3.5×10^5 e-h pairs in the bulk material under the assumption of an average eh-pair creation energy of $13.5\,\mathrm{eV}$. At the lowest absolute applied bias voltage ($100\,\mathrm{V}$ or $-100\,\mathrm{V}$), the detector capacity is charged with $2 \times 10^{-10}\,\mathrm{C}$ on the electrodes, or $1.24 \times 10^9\,e$ which is much larger than the number of induced e-h pairs per α particle. Hence, we measure in the space-charge-free (SCF) regime for all applied voltages.

A $2\,\mathrm{GHz}$, two-staged, bipolar transistor amplifier with an amplification factor of $A_{\mathrm{amp}} = (138 \pm 7)$ at $3.3\,\mathrm{pF}$ input capacitance, a rms noise at the output of $\sigma = 2.8\,\mathrm{mV}$ at $3\,\mathrm{GHz}$ bandwidth, and an input resistance of $R_{\mathrm{in}} = 55\,\Omega$ amplifies the signal before it is read out via an oscilloscope. The amplifier — specifically built for diamond applications — has been tested and characterised prior to the measurements with test pulses of known amplitude and width. It shows a linear behaviour in the tested range from $10\,\mu\mathrm{V}$ up to $1000\,\mu\mathrm{V}$ input amplitude. The minimum resolvable rise time with a $2\,\mathrm{GHz}$ amplifier is $180\,\mathrm{ps}$. The cut-off frequency at $-3\,\mathrm{dB}$ within a RC-circuit is $f_c = 1/(2\pi R_{in}C_d) \approx 1\,\mathrm{GHz}$. The diamond is discharged over a $1.5\,\mathrm{m}$ long UT-85 cable, which has a very high analogue bandwidth. Hence, the amplifier is fast enough to resolve fast signal rise times coming from the detector. The read-out is realised via a LeCroy Wave-Pro 7300A with $3\,\mathrm{GHz}$ analogue bandwidth at a digitalisation rate of $10\,\mathrm{GS/s}$. Note that no bandwidth limitation or filtering has been used.

2.4. Data Taking and Analysis of Detector Response

The oscilloscope records individual pulses when the pulse amplitude exceeds a threshold of $10\,\mathrm{mV}$ in coincidence with a signal width $> 1\,\mathrm{ns}$. The combination of the two conditions reduces the trigger rate
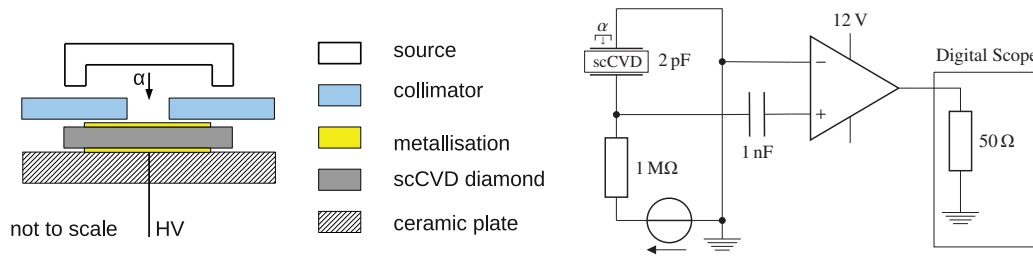
---

^{2}Diamond-Like Carbon

Figure 1. Sketch of the measurement set-up **(left)** and schematics of the α-TCT set-up **(right)**.

of detector noise induced triggers to effectively zero without cutting any signal whilst maintaining a short measurement duration of a few minutes per voltage-temperature pair. For an α-TCT signal with width < 1 ns a drift velocity of 50×10^6 cm/s would be required, which is much larger than the saturation velocity of not more than 12.5×10^6 cm/s at room temperature.

1000 pulses have been recorded for every given pair of temperature and bias voltage setting. Between two voltage settings, the HV has been turned off for one minute. After a temperature change sufficient time has been allowed to pass until the temperature has stabilised.

In the offline analysis the individual signals are corrected for trigger jitter and combined to form an average pulse. Only signals with a signal-to-noise ratio > 4 have been considered in order to reject pick-up triggers.[3] This selection rejects less then 1% of the pulses, i.e. of the order of 990 have been used per temperature-voltage pair.

The influence of integration effect of the sensor capacitance has been evaluated. For this, measured voltage pulses $u_m(t)$ have been translated into current pulses $i_m(t)$ and corrected for the integration effect using

$$i_m(t) = \frac{1}{A_{amp} R_{in}} \left[R_{in} C_d \frac{du_m(t)}{dt} + u_m(t) \right] . \tag{1}$$

The difference between input capacitance corrected current pulses and non-corrected current pulses is negligible. The correction term has thus been omitted.

In order to determine the transit time $t_t = t_e - t_s$, where t_s (t_e) denotes the start (end) time of drift, an error function (Erf) is fitted to both the rising and falling edge. The 50% points mark t_s and t_e, respectively.

For verification of the set-up, published results obtained with a scCVD diamond (*CVD2*, cf. [11]) have been compared to results obtained with our set-up using the *CVD2* diamond sample. The published pulse widths agree within 2% with the pulse widths measured with the set-up used here.

3. Induced Pulses from Carrier Movement

Hole (Fig. 2) and electron (Fig. 3) induced current have been recorded within a time window of 50 ns for the temperatures $T = 295, 250, 200, 150, 140, 125, 110, 100, 80, 67$ K. For hole pulses a bias voltage range $100 \text{ V} \leq |U_{bias}| \leq 400$ V in steps of 50 V was chosen, for electrons $100 \text{ V} \leq U_{bias} \leq 600$ V in steps of 100 V.

For temperatures $T \geq 150$ K fast rise times (< 2 ns) are seen for both hole and electron pulses. The duration of the rise times are field dependent. Higher electric field strengths lead to shorter rise times. As the minimal rise time of the amplifier is 180 ps, the observed shape of the rising edge is not limited by electronics, but characterises the successive start of drift of charge carriers. We attribute the strong dependence of the rise time on the electric field to the high charge density within the charge cloud produced by the α particle. Similarly, higher bias voltages lead to shorter fall times. This is to be expected as higher

---

[3]Pick-up is for example produced by other equipment in the laboratory as climate chambers, fridges, etc.

field strengths cause the free charge carriers to drift faster to the opposite electrode leading to shorter pulse durations, and hence less diffusion.

The rising edge of the signal marks the start of the charge drift. The falling edge marks the collection of charges at the opposite electrode. It should be mentioned that the initial distribution of the charge cloud has an effect on the signal edges.

At RT the signal has an almost flat top during the drift as a consequence of the field being constant over the diamond. In turn, this means that the net space-charge is very small. A net space-charge of the order of $\sim 10^{11}$ e/cm^3 already leads to a significant change in pulse shape, i.e. an exponential current behaviour [11]. Such intrinsic net space-charge seems to be absent in our sample. For a fixed voltage the pulses become shorter with decreasing temperature due to higher carrier mobility as phonon scattering decreases with decreasing temperature, see Sec. 4.

The pulse shape is noticeably dependent on the temperature for $T < 150$ K. The rising edge develops an $1 - \exp{(-t/\tau)}$ behaviour while the falling edge develops a long exponentially falling tail. We attribute these features to a retaining-releasing mechanism, in which charges are retained inside the initial high density charge cloud — produced by the α particle — and then released after a certain time.

Note that at RT the decrease in pulse width with increasing bias voltage is much more pronounced than at colder temperatures. For hole pulses at RT the difference in transit time Δt_t for 150 V and 400 V, normalized to the transit time at 400 V, is $r(295 \text{ K}) = \frac{\Delta t_t}{t_t(400)} \approx 0.7$ whereas at 67 K $r(67 \text{ K}) = \frac{\Delta t_t}{t_t(400)} \approx 0.2$.

The recorded current does not drop to zero after all charges have been collected but rather undershoots slightly. This can be explained by the AC-coupling of the detector to the current amplifier. Furthermore, the amplitude of the undershoot correlates with the total induced signal, hence at temperatures smaller than 150 K the undershoot decreases with decreasing temperature.

4. Temperature Dependence of Drift Mobility and Drift Velocity

The recorded signal is induced by the sum of the drifting carriers. Hence the measured transit time is the average over their entity. The measurement of the transit time allows us to calculate the average drift velocity

$$\langle v_{\text{drift}}(E) \rangle = d / t_t(E) \tag{2}$$

which increases with increasing electric field. We omit the indication of averaging hereafter. The Drude model of transport properties of electrons in materials [18] predicts a linear dependence of the drift velocity on the electric field $v_{\text{drift}} = \mu_0 E$. It is well known that this only holds true for low field strengths. With increasing fields the drift velocity saturates against v_{sat} as the carriers acquire more energy from the field in between scattering processes and hence obtain a higher effective temperature than the lattice. This results in frequent emission of optical phonons [19]. Hence, we use the field dependent drift mobility [20]

$$\mu(E) = \frac{\mu_0}{1 + \dfrac{\mu_0 E}{v_{\text{sat}}}} \, , \tag{3}$$

where μ_0 is the low-field mobility, leading to

$$v_{\text{drift}}(E) = \mu(E)E \, . \tag{4}$$

The model reduces to the Drude model at low fields ($\mu \rightarrow \mu_0$). It incorporates a saturation velocity for high fields, which are usually present in diamond detector applications.

Fig. 4 shows the average drift velocity for holes (left) and electrons (right) as a function of the electric field for various temperatures. The values are obtained from data using Eq. (2). The average drift velocity is not directly proportional to the field strength. For holes a drift velocity of $(7.39 \times 10^6 \pm 0.13 \times 10^6)$ cm/s and for electrons of $(5.21 \times 10^6 \pm 0.22 \times 10^6)$ cm/s at ∓ 0.8 V/μm is measured at RT. The drift velocity rises for a constant bias voltage with decreasing temperature. It also increases for a given temperature with increasing bias voltage; the asymptote yielding the saturation velocity. Eq. (4) is fitted to the drift velocity data for fixed
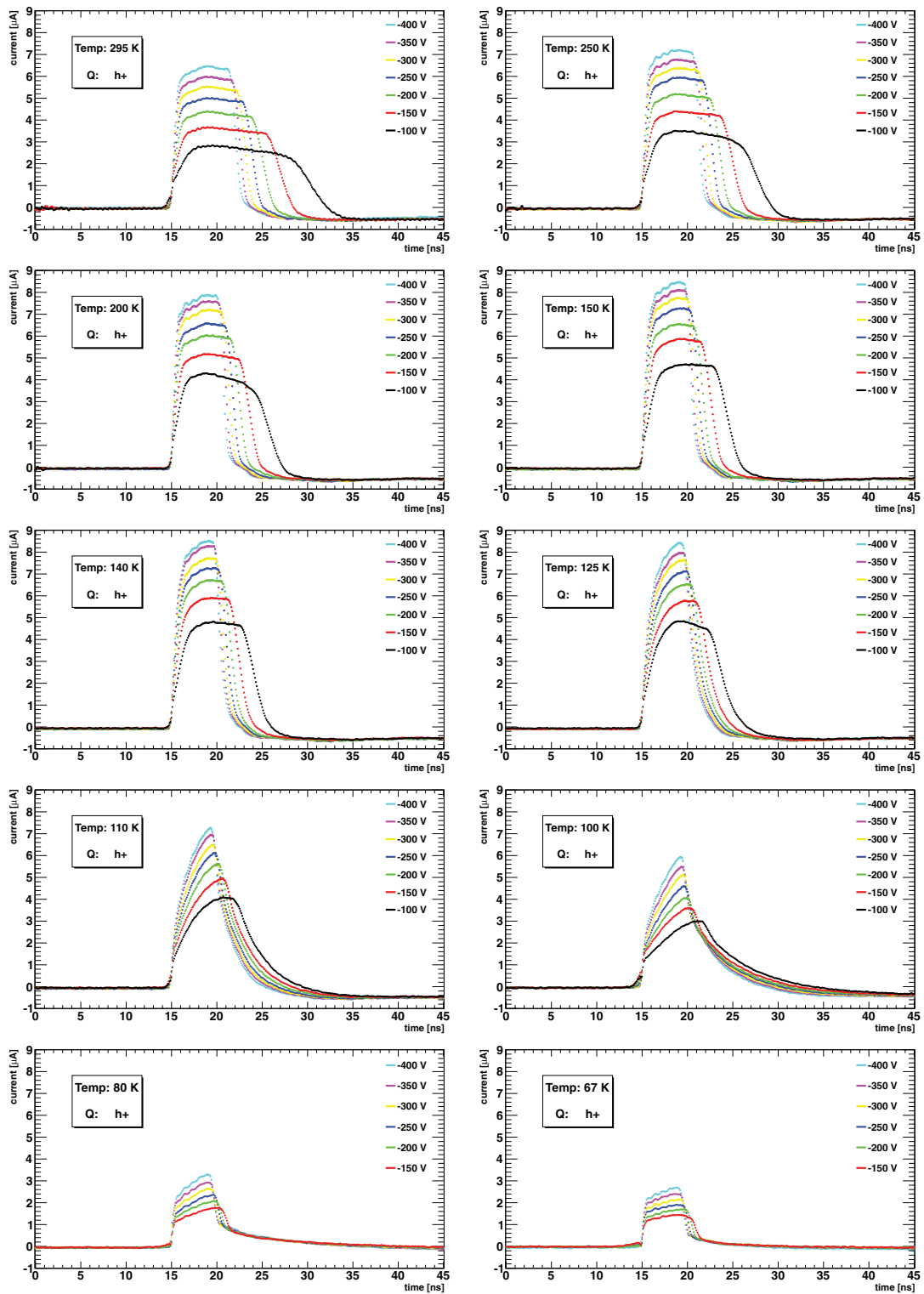
Figure 2. Diamond current pulses for holes at various temperatures and bias voltages.
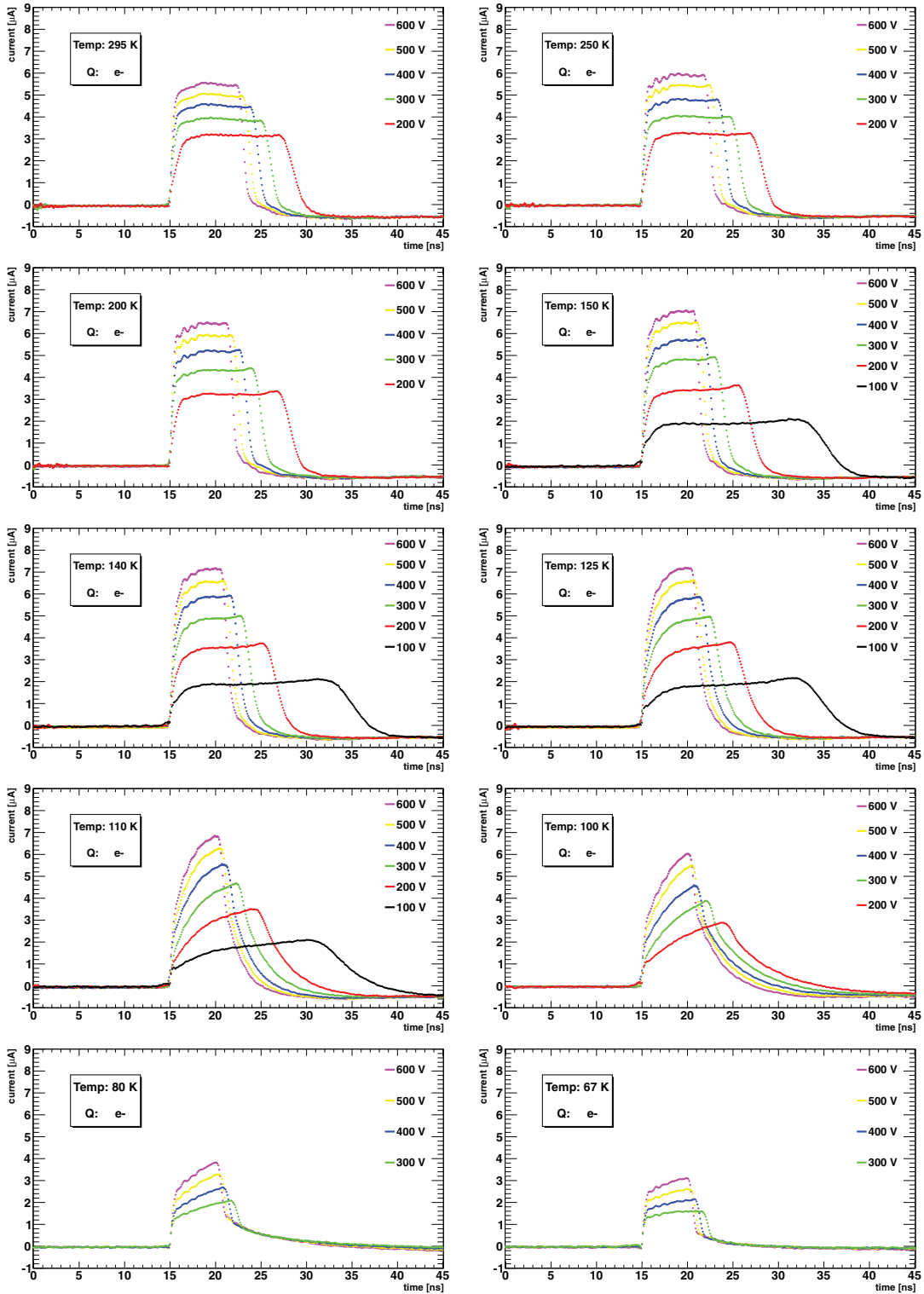
Figure 3. Diamond current pulses for electrons at various temperatures and bias voltages.
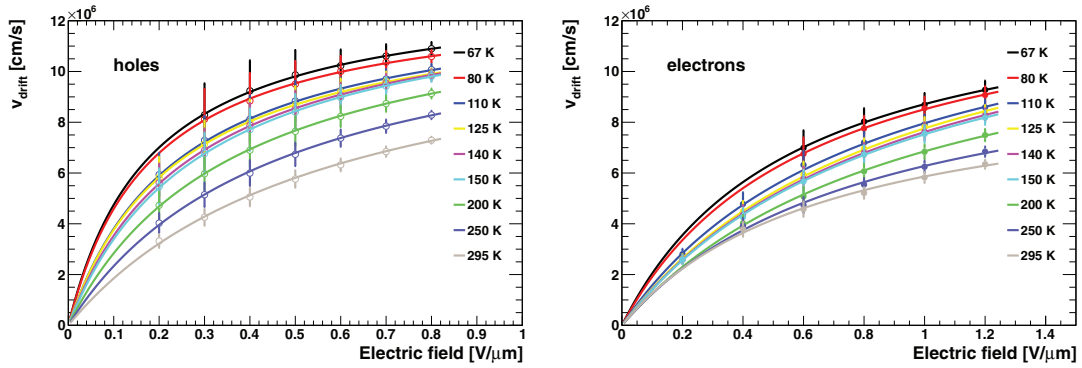
Figure 4. The average drift velocity against the electric field for different temperatures. The solid lines are fits after Eq. 4.
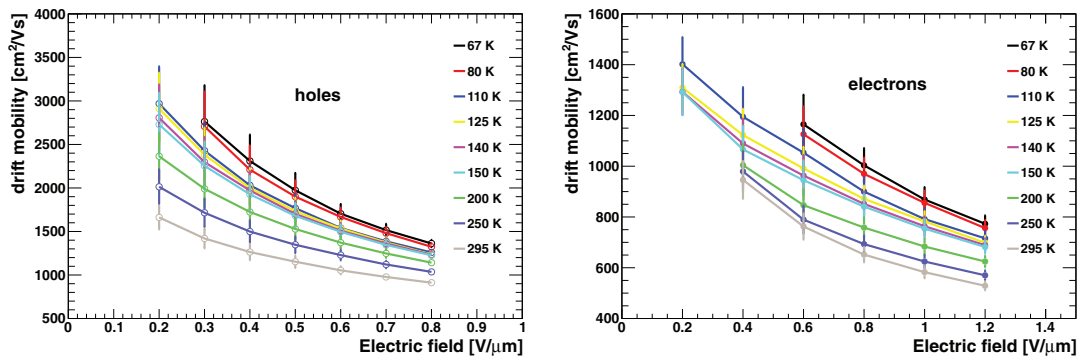

Figure 5. The drift mobility after Eq. 5 against the electric field for various temperatures. The solid lines serve as guide for the eye.

temperatures. Good agreement is observed. Each fit yields μ_0 and v_{sat} for a given temperature. The low-field mobility μ_0 increases with decreasing temperature, as is expected from diminishing phonon scattering. The fits result in low-field mobility values for holes at RT and at 67 K of $\mu_{0,h}(295\,\text{K}) = (2280 \pm 110)\,\text{cm}^2/\text{Vs}$ and $\mu_{0,h}(67\,\text{K}) = (7300 \pm 1850)\,\text{cm}^2/\text{Vs}$, respectively. The obtained results are in agreement with [11],[14]; values obtained in [13] cannot be reproduced. For electrons we find $\mu_{0,e}(295\,\text{K}) = (1440 \pm 220)\,\text{cm}^2/\text{Vs}$ and $\mu_{0,e}(67\,\text{K}) = (2400 \pm 840)\,\text{cm}^2/\text{Vs}$. Saturation velocity values for holes are $v_{sat,h}(295\,\text{K}) = (12.5 \times 10^6 \pm 1.1 \times 10^6)\,\text{cm/s}$ and $v_{sat,h}(67\,\text{K}) = (13.4 \times 10^6 \pm 1.5 \times 10^6)\,\text{cm/s}$, and for electrons $v_{sat,e}(295\,\text{K}) = (9.9 \times 10^6 \pm 1.1 \times 10^6)\,\text{cm/s}$ and $v_{sat,e}(67\,\text{K}) = (13.7 \times 10^6 \pm 2.7 \times 10^6)\,\text{cm/s}$.

We calculate the drift mobility for a certain bias voltage as

$$\mu = \frac{v_{drift}(E)}{E} = \frac{d}{E\,t_t(E)} \ . \tag{5}$$

Fig. 5 shows the drift mobility as a function of the electric field. It monotonically decreases with higher field strength as usually observed in semiconductors. Our adopted fitting model seems to be non-optimal for the particular shapes of the TCT pulses at 100 K leading to biased results, overestimating the transit time. The fit results for 100 K are therefore omitted for the rest of the paper.

We further discuss the temperature dependence of the low-field mobility. At high temperatures – around 300 K – the low-field mobility limited by acoustic phonon scattering (aps) follows a behaviour like $\mu \propto T^\alpha$ with $\alpha = -3/2$ [21]. But as other scatter mechanisms occur additionally, deviations from this theoretical value are observed in various materials, e.g. $\alpha = -2.2$ in p-type Si and $\alpha = -1.0$ in n-type GaAs.

The low-field mobility μ_0 for the SUT as a function of temperature on double-logarithmic scale is shown in Fig. 6. For holes (open circles), it increases with decreasing temperature over the scanned temperature
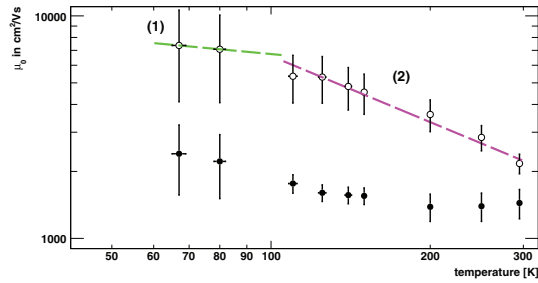
Figure 6. The low-field mobility from effective mobility fits plotted against temperature on double-logarithmic scale.

range down to 100 K and remains about constant for lower temperatures. In the case of electrons (full circles), this behaviour is not as clear. It seems to slightly rise from 150 K down to 67 K. For 150 K to 295 K the low-field mobility rises again. The double-logarithmic scale is chosen as a polynomial dependence of μ_0 on the temperature is expected. A fit $\mu(T) = \mu_0 \left(\frac{T}{300\,\text{K}}\right)^{\alpha}$ is performed in the region 105 K to 300 K (1) and 60 K to 105 K (2) for the hole low-field mobility. We find $\alpha^{(1)} = -0.99 \pm 0.17$ and $\alpha^{(2)} = -0.22 \pm 0.7$, where $\alpha^{(2)}$ is compatible with zero. Our results in region (1) clearly differ from the theoretical prediction.

The measured $\alpha^{(2)}$ is larger than $\alpha^{(1)}$. At lower temperatures the scattering of charge carriers off acoustic phonons is reduced and scattering off crystal impurities might play a dominant role. Theoretically the scattering off ionized impurities depends on the temperature with $\alpha = 3/2$ [22], whereas for non-ionized impurity scattering (niis) different models are found in the literature. Sclar [23] finds $\alpha^{\text{niis}} = 1/2$, Ansel'm [24] $\alpha^{\text{niis}} = -1/2$, and Erginsoy [25] $\alpha^{\text{niis}} = 0$. We assume non-ionized impurities to be the present situation. A transition from α^{aps} to α^{niis} might happen resulting in increasing values for α with decreasing temperatures. $\alpha^{(2)}$ could be interpreted as being the effective value for the transition region between two temperature regions where the mobility is either dominated by acoustic phonon scattering or non-ionized impurity scattering. A final conclusion cannot be made at this point as the uncertainty on μ_0 for the three lowest measured temperatures is too large. Further studies at higher and lower temperatures are planned in order to measure the exponent of the temperature dependence of low-field mobility in scCVD diamond for a wider temperature range.

The evolution of the second fit parameter v_{sat} with temperature is shown in Fig. 7 for holes (left) and electrons (right). v_{sat} seems to rise slightly between 295 K down to 150 K and then stabilises at $(13.2 \times 10^6 \pm 0.5 \times 10^6)$ cm/s for holes and $(14.6 \times 10^6 \pm 0.6 \times 10^6)$ cm/s for electrons. The values found are in good agreement with results reported earlier in [11] and the found temperature dependence agrees with theoretical predictions.
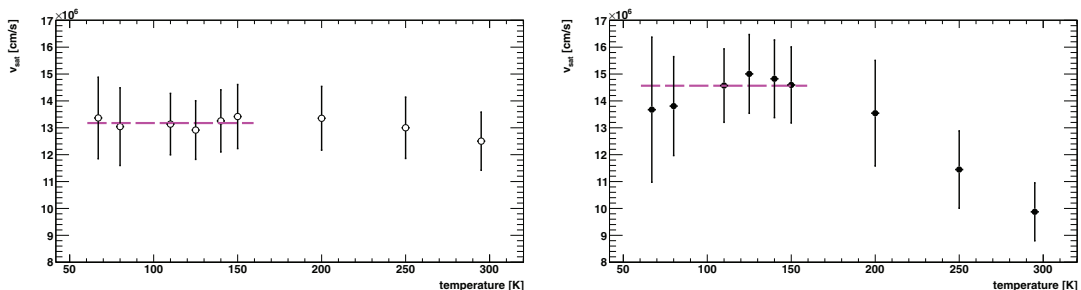

Figure 7. The saturation velocity from effective mobility fits plotted against temperature. Note the zero-suppression of the y-axis.

5. Conclusion

We have presented α-TCT measurements on a scCVD carried out over a temperature range from room temperature down to $67\,\text{K}$ and an electric field range from $-0.2\,\text{V/\mu m}$ to $-0.8\,\text{V/\mu m}$ for holes and from $0.2\,\text{V/\mu m}$ to $1.2\,\text{V/\mu m}$ for electrons. The temperature dependence of the low-field mobility and saturation velocity has been studied. We have found the saturation velocity for holes in scCVD diamond towards low temperatures to be $(13.2 \times 10^6 \pm 0.5 \times 10^6)\,\text{cm/s}$ and $(14.4 \times 10^6 \pm 0.6 \times 10^6)\,\text{cm/s}$ for electrons. Values for the low-field mobility for holes of $\mu_{0,h}(295\,\text{K}) = (2280 \pm 110)\,\text{cm}^2/\text{Vs}$ and $\mu_{0,h}(67\,\text{K}) = (7300 \pm 1850)\,\text{cm}^2/\text{Vs}$ and for electrons of $\mu_{0,e}(295\,\text{K}) = (1440 \pm 220)\,\text{cm}^2/\text{Vs}$ and $\mu_{0,e}(67\,\text{K}) = (2400 \pm 840)\,\text{cm}^2/\text{Vs}$ have been measured. Assuming $\mu(T) = \mu_0 \left(\frac{T}{300\,\text{K}}\right)^\alpha$, the exponent of the temperature dependence of the low-field drift mobility between $295\,\text{K}$ and $105\,\text{K}$ has been fitted to $\alpha = -0.99 \pm 0.17$. The temperature and voltage dependence of the total signal charge as well as further studies of the pulse shape are currently ongoing.

References

[1] The CMS Experiment at the CERN Large Hadron Collider, Journal of Instrumentation 3 (08) (2008) S08004.
[2] The ATLAS Experiment at the CERN Large Hadron Collider, Journal of Instrumentation 3 (08) (2008) S08003.
[3] L. Evans, P. Bryant, The LHC Machine, Journal of Instrumentation 3 (08) (2008) S08001.
[4] A. Bell, E. Castro, R. Hall-Wilton, W. Lange, W. Lohmann, A. Macpherson, M. Ohlerich, N. Rodriguez, V. Ryjov, R. Schmidt, R. Stone, Fast beam conditions monitor BCM1F for the CMS experiment, Nuclear Instruments and Methods in Physics Research Section A: Accelerators, Spectrometers, Detectors and Associated Equipment 614 (3) (2010) 433 – 438.
[5] V. Cindro, D. Dobos, I. Dolenc, H. Frais-Klbl, A. Gorisek, E. Griesmayer, H. Kagan, G. Kramberger, B. Macek, I. Mandic, M. Mikuz, M. Niegl, H. Pernegger, D. Tardif, W. Trischuk, P. Weilhammer, M. Zavrtanik, The ATLAS Beam Conditions Monitor, Journal of Instrumentation 3 (02) (2008) P02004.
[6] B. Dehning, E. Effinger, D. Dobos, H. Pernegger, E. Griesmayer, Diamond Detectors as Beam Monitors, Tech. Rep. CERN-BE-2011-001, CERN, Geneva (May 2010).
[7] J. Koike, D. M. Parkin, T. E. Mitchell, Displacement threshold energy for type IIa diamond, Applied Physics Letters 60 (12) (1992) 1450 –1452.
[8] Koizumi, Physics and Applications of CVD Diamonds.
[9] M. Lampert, P. Mark, Current Injection in Solids.
[10] V. Eremin, N. Strokan, E. Verbitskaya, Z. Li, Development of transient current and charge techniques for the measurement of effective net concentration of ionized charges (Neff) in the space charge region of p-n junction detectors, Nuclear Instruments and Methods in Physics Research Section A: Accelerators, Spectrometers, Detectors and Associated Equipment 372 (3) (1996) 388 – 398.
[11] H. Pernegger, S. Roe, P. Weilhammer, V. Eremin, H. Frais-Kölbl, E. Griesmayer, H. Kagan, S. Schnetzer, R. Stone, W. Trischuk, D. Twitchen, A. Whitehead, Charge-carrier properties in synthetic single-crystal diamond measured with the transient-current technique 97 (7) (2005) 073704.
[12] J. Fink, P. Lodomez, H. Krüger, H. Pernegger, P. Weilhammer, N. Wermes, TCT characterization of different semiconductor materials for particle detection, Nuclear Instruments and Methods in Physics Research Section A: Accelerators, Spectrometers, Detectors and Associated Equipment 565 (1) (2006) 227 – 233.
[13] J. Isberg, A. Lindblom, A. Tajani, D. Twitchen, Temperature dependence of hole drift mobility in high-purity single-crystal CVD diamond, physica status solidi (a) 202 (11) (2005) 2194–2198.
[14] M. Nesladek, A. Bogdan, W. Deferme, N. Tranchant, P. Bergonzo, Charge transport in high mobility single crystal diamond, Diamond and Related Materials 17 (7-10) (2008) 1235 – 1240, proceedings of Diamond 2007, the 18th European Conference on Diamond, Diamond-Like Materials, Carbon Nanotubes, Nitrides and Silicon Carbide.
[15] http://www.nist.gov/pml/data/star/index.cfm.
[16] Diamond Detectors Ltd, 16 Fleetsbridge Business Centre, Upton Road, Poole, Dorset, BH17 7AF.
[17] J. Härkönen, The Cryogenic Transient Current Technique (C-TCT) measurement setup of CERN RD39 Collaboration, Nuclear Instruments and Methods in Physics Research A581 (2007) 347-350.
[18] P. Drude, Zur Elektronentheorie der Metalle, Annalen der Physik 306 (1900) 566–613.
[19] S. Sze, K. N. Kwok, Physics of Semiconductor Devices; 3rd ed., Wiley, Hoboken, NJ, 2007.
[20] Z. Li, H. Kraner, Modeling and simulation of charge collection properties for neutron irradiated silicon detectors, Nuclear Physics B - Proceedings Supplements 32 (1993) 398 – 409.
[21] J. Bardeen, W. Shockley, Deformation Potentials and Mobilities in Non-Polar Crystals, Phys. Rev. 80 (1950) 72–80.
[22] E. Conwell, V. F. Weisskopf, Theory of Impurity Scattering in Semiconductors, Phys. Rev. 77 (1950) 388–390.
[23] N. Sclar, Neutral Impurity Scattering in Semiconductors, Phys. Rev. 104 (1956) 1559–1561.
[24] A. I. Ansel'm, J. Exptl. Theoret. Phys. (U.S.S.R.) 24 (1953) 85.
[25] C. Erginsoy, Neutral Impurity Scattering in Semiconductors, Phys. Rev. 79 (1950) 1013–1014.